Pressure-dependent phase transitions in hybrid improper ferroelectric Ruddlesden-Popper oxides

Gabriel Clarke [1], Dominik Daisenberger [2], X. Luo,[3] S. W. Cheong,[3,4] Nicholas C. Bristowe,[5] and Mark S. Senn [1,*]

[1]*Department of Chemistry, University of Warwick, Gibbet Hill, Coventry CV4 7AL, United Kingdom*
[2]*Diamond Light Source Ltd, Harwell Science and Innovation Campus, Didcot OX11 0DE, United Kingdom*
[3]*Laboratory for Pohang Emergent Materials, Pohang Accelerator Laboratory and Max Plank POSTECH Center for Complex Phase Materials, Pohang University of Science and Technology, Pohang 790-784, Korea*
[4]*Rutgers Center for Emergent Materials and Department of Physics & Astronomy, Rutgers University, Piscataway, New Jersey 08854, USA*
[5]*Centre for Materials Physics, Durham University, South Road, Durham DH1 3LE, United Kingdom*

The temperature-dependent phase transitions in Ruddlesden-Popper oxides with perovskite bilayers have been under increased scrutiny in recent years due to the so-called hybrid improper ferroelectricity that some chemical compositions exhibit. However, little is currently understood about the hydrostatic pressure dependence of these phase transitions. Herein we present the results of a combined high-pressure powder synchrotron x-ray diffraction experiment and *ab initio* study on the bilayered Ruddlesden-Popper phases $Ca_3Mn_2O_7$ and $Ca_3Ti_2O_7$. In both compounds we observe a first-order phase transition, that in combination with our density functional theory calculations, we can confidently assign as being between polar $A2_1am$ and nonpolar $Acaa$ structures. Interestingly, we show that while the application of pressure ultimately favors a nonpolar phase, as is commonly observed for proper ferroelectrics, regions of response exist where pressure actually acts to increase the polar mode amplitudes. The reason for this can be untangled by considering the varied response of octahedral tilts and rotations to hydrostatic pressure and their trilinear coupling with the polar instability.

I. INTRODUCTION

Ferroelectric (FE) materials have been widely studied for their technological applications in sensing, memory devices, and beyond [1]. Understanding structural distortions in functional properties under different conditions is crucial in determining the usability of a given material for a particular device. FE phase transitions are generally well understood as functions of temperature or chemical doping, with the $Pb(Ti/Zr)O_3$ [2–4] and $BaTiO_3$ [5–10] perovskites (and solid solutions related to them) enjoying a great deal of attention. These materials fall under the class of "proper" FEs, as the induction of a spontaneous, switchable polarization is a primary order parameter (OP) of the FE phase transition. Upon the application of pressure, proper FEs tend to undergo phase transitions to nonpolar structures. For example, $BaTiO_3$ transitions from a tetragonal FE phase to a cubic paraelectric (PE) phase at 2 GPa at 300 K [11].

However, structural types that exhibit proper FEs comprise only a fraction of all polar materials. Improper FE occurs when the polarization is a secondary OP of the FE phase transition [12,13]. In the specific case of hybrid improper

ferroelectricity (HIF), the primary order parameter is a pair of nonpolar octahedral distortions. These couple to a polar mode in a trilinear coupling mechanism; the polarization is inhibited if the amplitudes of either of the nonpolar distortions or the polar mode are reduced [14]. HIF is of particular interest in multiferroic research due to its breaking of the "d^0 rule," broadening the library of potential materials to those which include magnetic d^n cations [15,16]. High-pressure studies of HIF materials are sparser than investigations into proper FE materials, with the $n = 2$ Ruddlesden-Popper (RP) $Ca_3Mn_2O_7$ and $Ca_3Ti_2O_7$, which are otherwise among the most-studied materials at ambient pressure [14,17–22], receiving relatively little attention. $Ca_3Mn_2O_7$ has been shown to be sensitive to pressure [23–25], with several experiments evidencing a phase transition from the polar $A2_1am$ phase to a nonpolar phase at around 1–1.3 GPa. We are not aware of any experimental work investigating the high-pressure phase transitions of $Ca_3Ti_2O_7$, and the mechanism by which pressure couples to polarization in these materials is not well understood.

We have previously shown [19] that $Ca_3Mn_2O_7$ exhibits a phase coexistence between the polar $A2_1am$ structure and the nonpolar $Acaa$ structure over a wide temperature range. The structural differences between these two phases can be visualized as distortions acting on the aristotype tetragonal $I4/mmm$ phase: the $A2_1am$ phase has undergone both an in-phase rotation of the oxide octahedra and an out-of-phase tilt (with irreps X_2^+ and X_3^-, respectively) which are coupled to a polar displacement with irrep Γ_5^-, whereas the $Acaa$ phase only exhibits an out-of-phase rotation of the octahedra

*m.senn@warwick.ac.uk

(the X_1^- mode). A visualization of these modes is shown in the Supplemental Material (Fig. S1) [26]. By contrast, we have recently shown [27] that $Ca_3Ti_2O_7$ exhibits a first-order phase transition between $A2_1am$ and $Acaa$. With doping by Sr, this switches to a continuous second-order transition at $Ca_{2.15}Sr_{0.85}Ti_2O_7$ [27]. This is made possible by a continuous decrease in the magnitude of the rotation mode associated with the TiO_6 octahedra, followed by a rotation in the order-parameter direction and decrease in magnitude of the tilt mode. We have recently attempted to probe the behavior of the distortion modes observed in $Ca_{2.15}Sr_{0.85}Ti_2O_7$ under the effect of an applied electric field, finding a subtle preference for the X_2^+ rotation mode to unwind rather than the X_3^- tilt mode [28]. These results, coupled with the results of the temperature-based investigations, strongly imply that the X_2^+ mode is the softer of the two for this phase.

In this work, we perform synchrotron powder x-ray diffraction experiments on $Ca_3Mn_2O_7$ and $Ca_3Ti_2O_7$, using a diamond anvil cell to achieve pressures in excess of 30 GPa. Our results show that, in conjunction with density functional theory (DFT) calculations, in both phases, at high pressures a centrosymmetric phase with a single condensed out-of-phase rotation (X_1^-) is recovered. However, our calculations show that, contrary to what is expected for proper FEs, the initial application of pressure actually enhances the polar mode in $Ca_3Ti_2O_7$. This result can be understood due to the fact that the octahedral rotations are enhanced at a greater rate than the octahedral tilts are suppressed, leading to an enhancement in the trilinear coupling term with the polarization.

II. EXPERIMENTAL DETAILS AND DATA ANALYSIS

For high-pressure powder diffraction experiments, the samples used in our previous variable temperature study [19] were loaded into LeToullec-style membrane diamond anvil cells (DACs) equipped with Boehler-Almax anvils with 400-μm culets. The gasket material was Re, preindented to about 50 μm, with a 200-μm EDM "drilled" hole to form the sample chamber. The pressure-transmitting medium was Ne, small ruby chips and some Cu were added as pressure gauges. The x-ray beam size was 70-μm round diameter. Powder x-ray diffraction measurements were performed at Beamline I15 at Diamond Light Source. The beam energy was approximately 29 keV, corresponding to a wavelength of 0.424 48(1) Å refined using a LaB_6 standard. Diffraction patterns were recorded at intervals as the pressure was increased up to a maximum of 39.86 GPa for $Ca_3Mn_2O_7$ and 38.48 GPa for $Ca_3Ti_2O_7$. Pawley refinements were performed against the data using TOPAS ACADEMIC v6 [29], in which we fit rather than subtract the background, as is the norm when performing such analysis. Due to extreme preferred orientation it was unfortunately not possible to perform Rietveld refinements. It is important to note also that the diamond anvils themselves enter reflection condition under certain pressures which are not easily avoidable in the limited 2θ accessible due the masking imposed by the DAC, across the large pressure range studied. Compressibility calculations for both phases were performed using the principal axis strain calculator PASCAL [30].

The DFT calculations on $Ca_3Ti_2O_7$ were performed using the Vienna *ab initio* simulation package (VASP), version
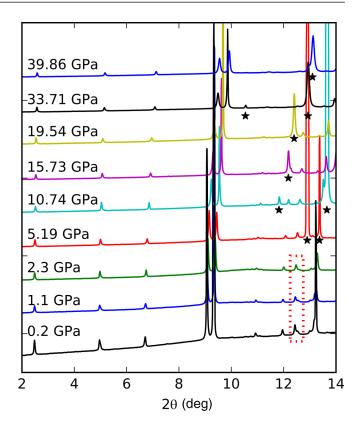

FIG. 1. Selected diffraction patterns recorded for $Ca_3Mn_2O_7$ at a variety of pressures. Diffraction artifacts resulting from the DAC are indicated by stars. The change from observing two (0 0 10) reflections (one each for the $A2_1am$ and $Acaa$ phases) to a single reflection for the $Acaa$ phase is indicated by the red dotted rectangle.

5.4.4 [31–34]. We employed the PBEsol exchange correlation potential and projector augmented-wave (PAW) pseudopotentials, as supplied within the VASP package [32,35,36]. A plane-wave basis set with a 700-eV energy cutoff and a $6 \times 6 \times 1$ Monkhorst-Pack k-point mesh with respect to the parent tetragonal primitive cell (scaled accordingly for other supercells) were found to be appropriate.

III. RESULTS AND DISCUSSION

We collected high-pressure powder diffraction patterns of $Ca_3Mn_2O_7$ and $Ca_3Ti_2O_7$ between 0 and 39.86 GPa. While it is difficult to differentiate the HIF phase $A2_1am$ and uniaxial negative thermal expansion (NTE) $Acaa$ phase using Pawley refinements alone, previous work [37] has shown that the $Acaa$ phase has a consistently longer c axis than the $A2_1am$ phase. Assuming that this holds true at the pressures over which we perform our experiment, we may assign the contributions of each phase to the diffraction patterns in Figs. 1 and 2. These assumptions are also consistent with the results of our DFT calculations presented later on. The occurrence of a phase transition can most easily be appreciated by considering the (0 0 10) reflection associated with the $A2_1am$ structure, which disappears around 1 GPa, although the small tail at the high-angle side of the (0 0 10) peak for the $Acaa$ phase indicates that a small amount of highly strained $A2_1am$ phase may persist above this pressure. This result is consistent
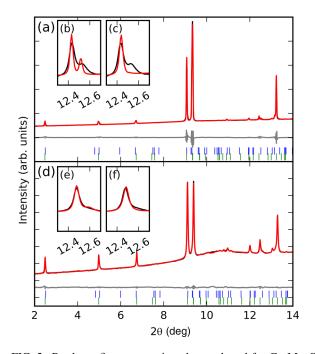
FIG. 2. Pawley refinement against data gathered for $Ca_3Mn_2O_7$ at (a) 0.2 GPa and (d) 2.3 GPa showing observed (black), calculated (red), and difference (gray) lines. Upper blue ticks indicate reflections for the $A2_1am$ phase, lower green ticks indicate reflections for the $Acaa$ phase. Insets (b) and (e) show the result of a two-phase refinement, showing an improved fit for the (0 0 10) peaks against insets (c) and (f), which show the result of a refinement including only an $Acaa$ phase.

with the phase coexistence reported in $Ca_3Mn_2O_7$ at room temperature and ambient pressure [37].

The lattice parameters extracted from Pawley refinements are plotted in Fig. 3, with an inset showing in detail how the two-phase system evolves up to 2 GPa. In contrast to
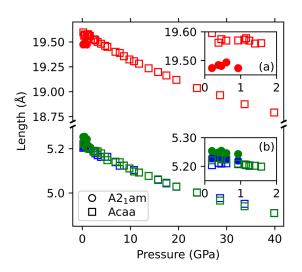

FIG. 3. Lattice parameters for $Ca_3Mn_2O_7$. Blue symbols indicate the a parameter, green symbols indicate the b parameter, and red symbols indicate the c parameter. Insets (a) and (b) show the 0–2 GPa regions of each part of the plot, showing detail of the two-phase system.
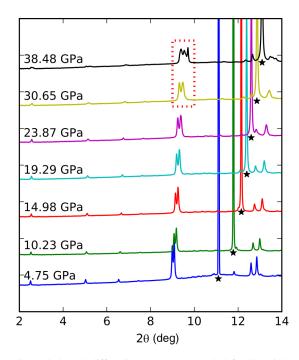

FIG. 4. Selected diffraction patterns recorded for $Ca_3Ti_2O_7$ at a variety of pressures. Diffraction artifacts resulting from the DAC are indicated by stars and the appearance of the (0 2 0) reflection for the $Acaa$ phase is indicated by the red dotted rectangle.

previous work [23], we do not find evidence for a tetragonal-orthorhombic phase transition at 1.3 GPa, nor an orthorhombic-tetragonal phase transition around 9.5 GPa. Instead, the behavior of the c parameter lends additional support to the dual-phase system at low pressure: single-phase refinements result in a deviation from linearity which is not apparent when the data are refined using the two-phase model described above.

In contrast to $Ca_3Mn_2O_7$, $Ca_3Ti_2O_7$ is well fit by a Pawley refinement with only a single $A2_1am$ phase between ambient pressure and the penultimate pressure point in this experiment (30.65 GPa). Above this pressure, additional reflections appear in the diffraction pattern which we fit by including an $Acaa$ phase. The reflection best suited to observing this secondary phase is (0 2 0), for this particular data set, as highlighted in Figs. 4 and 5. The (0 0 10) reflection is not consistently usable in this case as it becomes contaminated by a reflection from the DAC (Fig. 6). The experimental and calculated lattice parameters for $Ca_3Ti_2O_7$ are shown in Fig. 7; they follow a generally linear trend through the aforementioned pressure regime before changing at 38.48 GPa. When extracted from a single-phase $A2_1am$ refinement, the a parameter exhibits an upturn at the maximum pressure, while the b and c parameters begin to show signs of plateauing in their otherwise linear decrease. The DFT-calculated $A2_1am$ lattice parameters agree qualitatively with the experimental results, with the a and b parameters only deviating at the maximum pressure point where there is a phase coexistence. The calculated c parameter is qualitatively similar to its experimental counterpart, though consistently shorter by approximately 0.1 Å, suggesting that ground-state DFT calculations overestimate the magnitude of the X_3^- octahe-
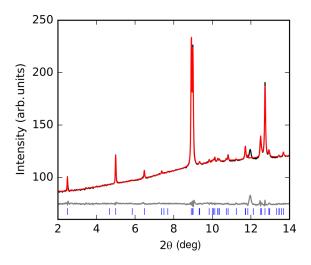
FIG. 5. Pawley refinement against data gathered for $Ca_3Ti_2O_7$ at near-ambient pressure, showing observed (black), calculated (red), and difference (gray) lines. Blue ticks indicate reflections for the $A2_1am$ phase. The small feature at $2\theta = 12°$ is a result of the diamond anvil cell fulfilling the diffraction condition.

FIG. 7. Lattice parameters for $Ca_3Ti_2O_7$. Blue symbols indicate the a parameter, green symbols indicate the b parameter, red symbols indicate the c parameter; dotted and dashed-dotted lines represent the calculated results for the $A2_1am$ and $Acaa$ phases, respectively.

dral tilt observed experimentally at ambient temperature. The calculated *Acaa* lattice parameters clearly do not agree well with the experiment between 0–30 GPa, indicating that this is not the correct structural model in this pressure regime. The a and b parameters are underestimated and the c parameter is calculated to be longer than the experimental results. However, a qualitative level of agreement across the $A2_1am$ to *Acaa* transition (with c becoming long and a and b shorter) between the experimentally assigned *Acaa* phase at 38.48 GPa and the DFT calculations is evident for the final pressure point of our experiment. The lack of a greater quantitative level of
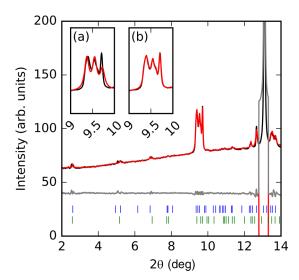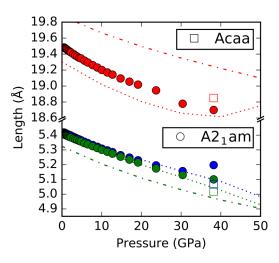

FIG. 6. Pawley refinement against data gathered for $Ca_3Ti_2O_7$ at 38.48 GPa, showing observed (black), calculated (red), and difference (gray) lines. Blue ticks indicate reflections for the $A2_1am$ phase. Inset (a) shows the result of a single-phase refinement in $A2_1am$, inset (b) shows the result of a two-phase refinement including an *Acaa* phase (green ticks). The feature at $2\theta = 13°$ is a result of the DAC fulfilling the diffraction condition.

agreement is most likely due to strong strain coupling arising from the intergrowth of coexisting $A2_1am$ and *Acaa* phases. A plot of the Lorentzian strain extracted from Pawley refinements on $Ca_3Ti_2O_7$ is shown in Fig. S2 [26], and shows how the phase transition acts to reduce the microstrain at elevated pressures. Unfortunately, due to experimental limits of the DACs, we were unable to study this sample at higher pressures where a single phase would most likely be realized. The experimental unit-cell volumes for $Ca_3Mn_2O_7$ and $Ca_3Ti_2O_7$ and calculated unit-cell volumes of the latter in $A2_1am$, *Acaa*, and $I4/mmm$ are shown in the Supplemental Material (Figs. S3 and S4) [26].

Compressibility parameters and Birch-Murnaghan coefficients were calculated using PASCAL [30] using the single-phase data for each composition: the data at pressures greater than 2.3 GPa for $Ca_3Mn_2O_7$ (*Acaa* structure) and all data below 30.65 GPa for $Ca_3Ti_2O_7$ ($A2_1am$ structure). These data are tabulated in the Supplemental Material (Tables S1 and S2) [26]. For both compositions, the principal axes are mapped directly on to the crystallographic axes as the tetragonal and orthorhombic structures both have orthogonal lattice vectors by definition. $Ca_3Mn_2O_7$ is less compressible along all axes (with higher bulk modulus) than $Ca_3Ti_2O_7$, possibly as a result of the structural differences between the *Acca* and $A2_1am$ phases. However, any comparisons between the results should be made with caution as the phase transition occurring for $Ca_3Mn_2O_7$ likely influences the accuracy with which the linear compressibility (extrapolated to zero pressure) is determined.

Figure 8(a) shows the calculated ground-state energies for the $A2_1am$ and *Acaa* phases of $Ca_3Ti_2O_7$ relative to the $I4/mmm$ phase up to 50 GPa. DFT finds the polar $A2_1am$ phase to be the ground state at 0 GPa, consistent with experimental observations. It can be seen that with increasing pressure, both the polar $A2_1am$ and nonpolar *Acaa* phases become increasingly stable with respect to the undistorted $I4/mmm$. However, the *Acaa* phase is stabilized with pressure at a much greater rate than the $A2_1am$ phase, and at
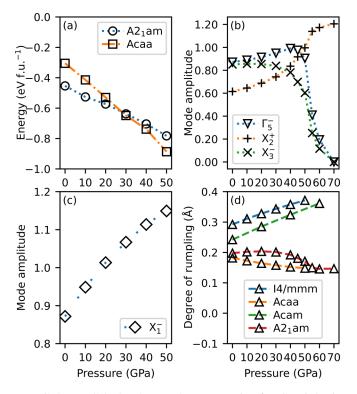
FIG. 8. (a) Calculated ground-state energies for $Ca_3Ti_2O_7$ in $A2_1am$ and $Acaa$ (relative to $I4/mmm$). (b), (c) Calculated mode amplitudes (A_p values as defined in ISODISTORT) for the $A2_1am$ and $Acaa$ structures of $Ca_3Ti_2O_7$. (d) Shows the calculated degree of rumpling for each phase as a function of pressure.

approximately 30 GPa it becomes more stable than the polar structure. This is in good agreement with our experimental results wherein we observe the phase transition in the 30.65–38.48 GPa range. The trend in the ground-state energies we find for the $A2_1am$ ($Cmc2_1$ standard setting) and $Acaa$ ($Ccce$) phases here are also qualitatively similar to those reported recently from a DFT study on $Sr_3Hf_2O_7$ [38], further strengthening our assignments. On the other hand, a recent synchrotron infrared spectroscopy experiment on HIF $Sr_3Sn_2O_7$ [39] has been interpreted based on more complex sequence of pressure-induced phase transitions at 2, 15, and 18 GPa than we observe in $Ca_3Ti_2O_7$. The first of these is the FE transition, which is assigned as first order as it resulted from a transition between two phases without a group-subgroup relationship: $A2_1am$ and $Pnab$. The $Pnab$ structure has also been investigated computationally as an important switching pathway in related HIFs [40]. The $Pnab$ structure still exhibits a trilinear coupling term, but instead of an in-phase X_2^+ rotation there is an out-of-phase X_1^- rotation of the oxide octahedra which now couples to antiferrodistortive M_5^+ mode in which the displacements of Sr^{2+} cations cancel one another within a perovskite block. To test this possible alternative sequence of phase transition we also relax $Ca_3Ti_2O_7$ within this $Pnab$ symmetry. However, over the pressure range 0 to 40 GPa, we find that our structures always relax back to a structure that has $Acaa$ symmetry (see Supplemental Material [26]). Thus, we discount this scenario for the specific composition we have studied here, and

note both the experimental and computational care that needs to be taken in distinguishing between phases of these two symmetries.

To understand the pressure-induced phase transitions in $Ca_3Ti_2O_7$ in greater detail, we decompose its DFT-relaxed $A2_1am$ and $Acaa$ structures in terms of symmetry-adapted displacements using ISODISTORT [41] [Figs. 8(b) and 8(c)]. For the $Acaa$ phases we observe a slow increase in the amplitude of the X_1^- modes up to 50 GPa, corresponding to the magnitude of the out-of-phase octahedral rotations increasing with pressure. The behaviors of the modes in the $A2_1am$ structure were calculated up to 70 GPa and are somewhat different; the X_2^+ in-phase rotation increases in amplitude with increasing pressure up to 40 GPa, while the X_3^- out-of-phase tilt mode remains constant up to 30 GPa before beginning to decrease in magnitude at 40 GPa. Surprisingly, contrary to what is normally found in proper FEs, the Γ_5^- polar mode that couples to both of these via a trilinear term in the free-energy expansion actually increases gradually in this regime. Above 40 GPa, the X_3^- begins to decrease in amplitude more rapidly, disappearing at 70 GPa, whereas the X_2^+ mode starts to increase more rapidly at this point. We show in Fig. S5 [26] that an uncoupled X_3^- distortion (with the space group $Acam$) increases in amplitude with applied pressure. The polar Γ_5^- mode starts to decreases in magnitude and then disappears finally at 70 GPa, as is to be expected since the trilinear term must necessarily vanish as the tilt magnitude (X_3^-) goes to zero. We emphasize here, although these results on the evolution of the octahedral tilting, rotation, and polar distortions are derived from our DFT calculations only, the good agreement between experiment and theory for lattice parameter trends and phase transition pressures are strongly indicative of the fact that our DFT calculations provide an adequate description of $Ca_3Ti_2O_7$ within the pressure ranges we report.

Figure 8(d) shows the degree of rumpling [42] of the Ca-O rocksalt-like layer in the $I4/mmm$, $Acaa$ (containing only a rotation distortion with irrep X_1^-), $Acam$ (containing only a tilt distortion with irrep X_3^-), and $A2_1am$ phases of $Ca_3Ti_2O_7$. The term rumpling refers to the loss of coplanarity between the Ca and O atoms in these layers and its magnitude is described by the Γ_1^+ distortion mode (that is already active in the $I4/mmm$ parent phase). The rumpling is greatest in the $I4/mmm$ phase and increases with pressure. A similar trend is borne out in the tilt-only $Acam$ phase, while the rumpling is reduced by the inclusion of octahedral rotations (as in the $A2_1am$ structure). These results are in line with a recent study by Zhang *et al.* [43] showing that, in $n = 2$ RPs, phases with only tilting distortions are observed for larger rumpling amplitudes. Inclusion of an octahedral rotation (or indeed considering the $Acaa$ phase with only octahedral rotations) leads to a dramatic suppression of the rumpling mode that is exaggerated with increasing pressure. The microscopic origin of this can be understood via the corkscrew mechanism that we have proposed previously [44–46] to explain the coupling between in-plane lattice parameter contraction, octahedral rotation, rocksalt layer rumpling, and out-of-plane lattice parameter extension, which provides an explanation of the NTE observed in the $Acaa$ phase of these materials [19,47].

To investigate the unexpected trend with pressure that leads to an increase in the polar Γ_5^- mode, we plot its amplitude
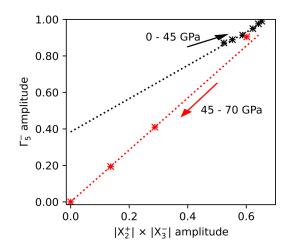
FIG. 9. Product of the calculated rotation and tilt mode amplitudes plotted against the calculated polar mode amplitude for $Ca_3Ti_2O_7$. The black and red dotted lines indicate the trends in the data below and above 45 GPa, respectively, showing how the calculated mode amplitudes deviate from the expected results due to the trilinear coupling mechanism below 30 GPa.

against that of ($|X_2^+| \times |X_3^-|$) (Fig. 9) in order to reveal to what extent this behavior is driven by the trilinear term [14]. Individual mode amplitudes are also included in the Supplemental Material (Figs. S7 and S8) [26]. This trend indicates that at low pressures the Γ_5^- amplitude is in excess of that expected from the trilinear mechanism, suggesting that there is a small, proper component in addition to that driven by the trilinear coupling. Only at much higher pressures above 45 GPa is a polarization magnitude consistent with that expected from the trilinear coupling (red line in Fig. 9) observed. This additional proper component to the polarization is confirmed via DFT calculations on an $F2mm$ phase that shows a Γ_5^- mode which has vanished by a pressure of 40 GPa (see Fig. S6 [26]).

Comparing our results with the temperature-dependent phase diagrams [19,27] from the literature we observe our results do not follow the usual trend that the application of high pressure serves to mimic the sequence of phase transitions observed on cooling. To the contrary, we find that both for $Ca_3Mn_2O_7$ and $Ca_3Ti_2O_7$, elevating the temperature and pressure induces the phase transition from polar $A2_1am$ to the centrosymmetric $Acaa$. The fact that both the $A2_1am$ and $Acaa$ phases of $Ca_3Ti_2O_7$ are stabilized simultaneously opposes also the normal paradigm observed for proper FE perovskites, where the *initial* application of hydrostatic pressure favors the more "ordered" and higher-symmetry ground state and hence behaves analogously to lowering of temperature [48–53]. However, it is important to note that in proper ferroelectrics, it has been predicted, and experimentally verified in $PbTiO_3$ [49,54], that at pressure above 45 GPa there is a reentrant-type phase transition from the initially pressure-induced centrosymmetric phase to another polar structure. The origin of these phenomena in proper ferroelectrics at much higher pressures is likely distinct from the initial increase in polarization we report here in improper ferroelectric $Ca_3Ti_2O_7$.

Until recently, relatively little work has been published on the high-pressure behaviors of improper FE materials [55–60], though with the advent of HIF materials in the last decade, a greater interest has been developing. Recently, *ab initio* high-pressure calculations by Ramkumar and Nowadnick [61] up to 20 GPa has been published on the $Ca_3Ti_2O_7$, $Sr_3Zr_2O_7$, and $Zr_3Sn_2O_7$ phases. All three phases adopt a HIF ground state with the same $A2_1am$ symmetry, but with variations in the details of their responses to increasing pressure. As with our findings, in $Ca_3Ti_2O_7$ a competition between the X_3^- tilt and the X_2^+ rotation is observed that can be rationalized as being due to the opposite signs of the coupling of these modes with strain. Although the majority of their study is restricted to the HIF phase only, they do find that the enthalpy of the $Acaa$ phase decreases at a faster rate with respect to the $A2_1am$ phase. However, as their calculations were limited to 20 GPa they stop short of the experimental and computational observation of a first-order phase transition that we report here which provides crucial insight as to how the evolution of hybrid order parameters can actually result in a enhancement of polarization at intermediate pressure regimes.

Recently, there has been a significant interest in using uniaxial pressure and strain to tune the electronic properties of Ruddlesden-Popper oxides, including superconductivity in the hole-doped La_2CuO_4 [62] and Sr_2RuO_4 [63,64]. It is clear here that understanding the interplay between strains and structural degrees of freedom is crucial. Of particular relevance to this work is isostructural and isosymmetric $Ca_3Ru_2O_7$ which is believed to exhibit the Rashbar effect [65] on account of its $A2_1am$ polar and metallic ground state. It has very recently been shown that uniaxial pressure has a pronounced interplay with its spin transitions [66], and it will therefore be of utmost interest to investigate the interplay between octahedral tilting, polar distortions, and the Rashbar effect in this and other polar metallic Ruddlesden-Popper oxides.

IV. CONCLUSION

The application of hydrostatic pressure to the $n = 2$ RP phases $Ca_3Mn_2O_7$ and $Ca_3Ti_2O_7$ has been shown to result in a phase transition from the polar $A2_1am$ structure to the nonpolar $Acaa$ structure via a first-order phase transition. These transitions occur at approximately 1 GPa for $Ca_3Mn_2O_7$ and above 30 GPa for $Ca_3Ti_2O_7$. *Ab initio* calculations performed for $Ca_3Ti_2O_7$ indicate that the effect of increasing pressure is not to destabilize the polar structure with respect to the undistorted paraelectric phase, as would be expected for a proper FE material. Instead, the rate at which the $Acaa$ phase is stabilized exceeds the rate for the $A2_1am$ phase, leading to a crossover in the ground-state energies at a pressure that is consistent with the experimentally observed transitions. Crucially, in the $A2_1am$ phase of $Ca_3Ti_2O_7$ we predict a regime where pressure actually acts to increase the overall magnitude of the polar mode. Our results highlight that the response of improper FEs to pressure can be quite different to the conventionally observed suppression of polarization observed in proper FEs. Consequently, unexplored possibilities exist for using hydrostatic pressure to control the polarization states and the Rashba effect in improper FEs.

Diffraction data and DFT-optimized structures are available as supporting information and may be accessed in [67].

ACKNOWLEDGMENTS

[1] J. F. Scott, Applications of modern ferroelectrics, Science **315**, 954 (2007).

[2] H. S. Bhatti, S. T. Hussain, F. A. Khan, and S. Hussain, Synthesis and induced multiferroicity of perovskite $PbTiO_3$; a review, Appl. Surf. Sci. **367**, 291 (2016).

[3] J. A. Sanjurjo, E. López-Cruz, and G. Burns, High-pressure Raman study of zone-center phonons in $PbTiO_3$, Phys. Rev. B **28**, 7260 (1983).

[4] N. Jaykhedkar, N. Tripathy, V. Shah, B. Pujari, and S. Premkumar, A comprehensive study of pressure dependent phase transitions in ferroelectric $PbTiO_3$, $PbZrO_3$ and $BaTiO_3$, Mater. Chem. Phys. **254**, 123545 (2020).

[5] M. Acosta, N. Novak, V. Rojas, S. Patel, R. Vaish, J. Koruza, G. A. Rossetti, and J. Rödel, $BaTiO_3$-based piezoelectrics: Fundamentals, current status, and perspectives, Appl. Phys. Rev. **4**, 041305 (2017).

[6] D. L. Decker and Y. X. Zhao, Dielectric and polarization measurements on $BaTiO_3$ at high pressures to the tricritical point, Phys. Rev. B **39**, 2432 (1989).

[7] P. Pruzan, D. Gourdain, J. C Chervin, B. Canny, B. Couzinet, and M. Hanfland, Equation of state of $BaTiO_3$ and $KNbO_3$ at room temperature up to 30 GPa, Solid State Commun. **123**, 21 (2002).

[8] E. V. Mejía-Uriarte, R. Y. Sato-Berrú, M. Navarrete, M. Villagrán-Muniz, C. Medina-Gutiérrez, C. Frausto-Reyes, and H. Murrieta S, Phase transition of polycrystalline $BaTiO_3$ at high-pressure detected by a pulsed photoacoustic technique, Meas. Sci. Technol. **17**, 1319 (2006).

[9] E. V. Mejía-Uriarte, R. Y. Sato-Berrú, M. Navarrete, O. Kolokoltsev, and J. M. Saniger, Determination of phase transition by principal component analysis applied to raman spectra of polycristalline $BaTiO_3$ at low and high temperature, J. Appl. Res. Technol. **10**, 57 (2012).

[10] U. D. Venkateswaran, V. M. Naik, and R. Naik, High-pressure Raman studies of polycrystalline $BaTiO_3$, Phys. Rev. B **58**, 14256 (1998).

[11] C. L. Bull, C. J. Ridley, K. S. Knight, N. P. Funnell, and A. S. Gibbs, Comprehensive determination of the high-pressure structural behaviour of $BaTiO_3$, Mater. Adv. **2**, 6094 (2021).

[12] A. P. Levanyuk and D. G. Sannikov, Improper ferroelectrics, Usp. Fiz. Nauk **112**, 561 (1974) [Sov. Phys.–Usp. **17**, 199 (1974)].

[13] V. Dvorak, Improper ferroelectrics, Ferroelectrics **7**, 1 (1974).

[14] N. A. Benedek and C. J. Fennie, Hybrid improper ferroelectricity: A mechanism for controllable polarization-magnetization coupling Phys. Rev. Lett. **106**, 107204 (2011).

[15] E. Bousquet, M. Dawber, N. Stucki, C. Lichtensteiger, P. Hermet, S. Gariglio, J.-M. Triscone, and P. Ghosez, Improper ferroelectricity in perovskite oxide artificial superlattices, Nature (London) **452**, 732 (2008).

[16] N. A. Benedek, A. T. Mulder, and C. J. Fennie, Polar octahedral rotations: A path to new multifunctional materials, J. Solid State Chem. **195**, 11 (2012).

[17] A. B. Harris, Symmetry analysis for the Ruddlesden-Popper systems $Ca_3Mn_2O_7$ and $Ca_3Ti_2O_7$, Phys. Rev. B **84**, 064116 (2011).

[18] E. A. Nowadnick and C. J. Fennie, Domains and ferroelectric switching pathways in $Ca_3Ti_2O_7$ from first principles, Phys. Rev. B **94**, 104105 (2016).

[19] M. S. Senn, A. Bombardi, C. A. Murray, C. Vecchini, A. Scherillo, X. Luo, and S. W. Cheong, Negative thermal expansion in hybrid improper ferroelectric Ruddlesden-popper perovskites by symmetry trapping, Phys. Rev. Lett. **114**, 035701 (2015).

[20] W. Zhao, Z. Li, Z. Wang, Y. Peng, L. Shi, W. Hua, J. Wang, L. Wang, W.-D. Fei, and Y. Zhao, Large room temperature electrocaloric effect in $PbZrO_3/Ca_3Mn_2O_7$ heterostructure, Acta Mater. **254**, 118989 (2023).

[21] P. Rocha-Rodrigues, I. P. Miranda, S. S. M. Santos, G. N. P. Oliveira, T. Leal, M. L. Marcondes, J. G. Correia, L. V. C. Assali, H. M. Petrilli, J. P. Araújo, and A. M. L. Lopes, Probing $Ca_3Ti_2O_7$ crystal structure at the atomic level: Insights from $^{111m}Cd/^{111}Cd$ PAC spectroscopy and *ab-initio* studies, arXiv:2402.09945.

[22] L. Miao, K.-E. Hasin, P. Moradifar, D. Mukherjee, K. Wang, S.-W. Cheong, E. A. Nowadnick, and N. Alem, Double-Bilayer polar nanoregions and Mn antisites in $(Ca, Sr)_3Mn_2O_7$, Nat. Commun. **13**, 4927 (2022).

[23] J. L. Zhu, L. C. Chen, R. C. Yu, F. Y. Li, J. Liu, and C. Q. Jin, Phase transition in layered perovskite-like manganate $Ca_3Mn_2O_7$ under high pressure, Int. J. Mod. Phys. B **15**, 2491 (2001).

[24] W. Zhu, L. Pi, Y. Huang, S. Tan, and Y. Zhang, La-doping and external pressure effects on the crystal structure of layered perovskite-like manganate $Ca_3Mn_2O_7$, Phys. Status Solidi A **194**, 159 (2002).

[25] F. Ye, J. Wang, J. Sheng, C. Hoffmann, T. Gu, H. J. Xiang, W. Tian, J. J. Molaison, A. M. dos Santos, M. Matsuda, B. C. Chakoumakos, J. A. Fernandez-Baca, X. Tong, B. Gao, J. W. Kim, and S.-W. Cheong, Soft antiphase tilt of oxygen octahedra in the hybrid improper multiferroic $Ca_3Mn_{1.9}Ti_{0.1}O_7$, Phys. Rev. B **97**, 041112(R) (2018).

[26] See Supplemental Material at http://link.aps.org/supplemental/10.1103/PhysRevB.109.094107 for a PDF containing 9 figures and 3 tables giving further details of the analysis of the diffraction data and DFT calculations, as a function of pressure. This includes the fitting of the equation of state, the evolution of distortion mode amplitudes and the relative stability of the different structural phases considered.

[27] F. Pomiro, C. Ablitt, N. C. Bristowe, A. A. Mostofi, C. Won, S.-W. Cheong, and M. S. Senn, From first- to second-order phase transitions in hybrid improper ferroelectrics through entropy stabilization, Phys. Rev. B **102**, 014101 (2020).

[28] G. Clarke, C. Ablitt, J. Daniels, S. Checchia, and M. S. Senn, In situ X-ray diffraction investigation of electric-field-induced switching in a hybrid improper ferroelectric, J. Appl. Crystallogr. **54**, 533 (2021).

[29] A. A. Coelho, *TOPAS* and *TOPAS-Academic*: An optimization program integrating computer algebra and crystallographic objects written in C + +: An, J. Appl. Crystallogr. **51**, 210 (2018).

[30] M. J. Cliffe and A. L. Goodwin, *PASCal*: a principal axis strain calculator for thermal expansion and compressibility determination, J. Appl. Crystallogr. **45**, 1321 (2012).

[31] G. Kresse and J. Hafner, *Ab initio* molecular dynamics for liquid metals, Phys. Rev. B **47**, 558 (1993).

[32] G. Kresse and J. Furthmüller, Efficient iterative schemes for *ab initio* total-energy calculations using a plane-wave basis set, Phys. Rev. B **54**, 11169 (1996).

[33] G. Kresse and J. Furthmüller, Efficiency of *ab-initio* total energy calculations for metals and semiconductors using a plane-wave basis set, Comput. Mater. Sci. **6**, 15 (1996).

[34] G. Kresse and J. Hafner, *Ab initio* molecular-dynamics simulation of the liquid-metalamorphous- semiconductor transition in germanium, Phys. Rev. B **49**, 14251 (1994).

[35] J. P. Perdew, A. Ruzsinszky, G. I. Csonka, O. A. Vydrov, G. E. Scuseria, L. A. Constantin, X. Zhou, and K. Burke, Restoring the density-gradient expansion for exchange in solids and surfaces, Phys. Rev. Lett. **100**, 136406 (2008).

[36] P. E. Blöchl, Projector augmented-wave method, Phys. Rev. B **50**, 17953 (1994).

[37] M. S. Senn, D. A. Keen, T. C. A. Lucas, J. A. Hriljac, and A. L. Goodwin, Emergence of long-range order in $BaTiO_3$ from local symmetry-breaking distortions, Phys. Rev. Lett. **116**, 207602 (2016).

[38] M. C. B. Barbosa, E. L. da Silva, P. N. Lekshmi, M. L. Marcondes, L. V. C. Assali, H. M. Petrilli, A. M. L. Lopes, and J. P. Araújo, Pressure-induced phase transformations of quasi-2D $Sr_3Hf_2O_7$, J. Phys. Chem. C **127**, 15435 (2023).

[39] K. A. Smith, S. P. Ramkumar, N. C. Harms, A. J. Clune, X. Xu, S.-W. Cheong, Z. Liu, E. A. Nowadnick, and J. L. Musfeldt, Revealing pressure-driven structural transitions in the hybrid improper ferroelectric $Sr_3Sn_2O_7$, Phys. Rev. B **104**, 064106 (2021).

[40] S. Li and T. Birol, Suppressing the ferroelectric switching barrier in hybrid improper ferroelectrics, npj Comput. Mater. **6**, 168 (2020).

[41] B. J. Campbell, H. T. Stokes, D. E. Tanner, and D. M. Hatch, *ISODISPLACE*: A web-based tool for exploring structural distortions, J. Appl. Crystallogr. **39**, 607 (2006).

[42] Y. Zhang, J. Wang, and P. Ghosez, Unraveling the suppression of oxygen octahedra rotations in $A_3B_2O_7$ Ruddlesden-popper compounds: Engineering multiferroicity and beyond, Phys. Rev. Lett. **125**, 157601 (2020).

[43] B. H. Zhang, Z. Z. Hu, B. H. Chen, X. Q. Liu, and X. M. Chen, Improved hybrid improper ferroelectricity in B-site substituted $Ca_3Ti_2O_7$ ceramics with a Ruddlesden-Popper structure, J. Appl. Phys. **128**, 054102 (2020).

[44] C. Ablitt, S. Craddock, M. S. Senn, A. A. Mostofi, and N. C. Bristowe, The origin of uniaxial negative thermal expansion in layered perovskites, npj Comput. Mater. **3**, 44 (2017).

[45] C. Ablitt, A. A. Mostofi, N. C. Bristowe, and M. S. Senn, Control of uniaxial negative thermal expansion in layered perovskites by tuning layer thickness, Front. Chem. **6**, 455 (2018).

[46] C. Ablitt, Understanding and Controlling Uniaxial Negative Thermal Expansion in Ruddlesden-Popper Oxides, Ph.D. thesis, Imperial College, London, 2019.

[47] M. S. Senn, C. A. Murray, X. Luo, L. Wang, F.-T. Huang, S.-W. Cheong, A. Bombardi, C. Ablitt, A. A. Mostofi, and N. C. Bristowe, Symmetry switching of negative thermal expansion by chemical control, J. Am. Chem. Soc. **138**, 5479 (2016).

[48] S. A. Hayward, S. A. T. T. Redfern, H. J. Stone, M. G. Tucker, K. R. Whittle, and W. G. Marshall, Phase transitions in $BaTiO_3$: A high-pressure neutron diffraction study, Z. Kristallogr.: Cryst. Mater. **220**, 735 (2005).

[49] P. E. Janolin, P. Bouvier, J. Kreisel, P. A. Thomas, I. A. Kornev, L. Bellaiche, W. Crichton, M. Hanfland, and B. Dkhil, High-pressure effect on $PbTiO_3$: An investigation by Raman and X-ray scattering up to 63 GPa, Phys. Rev. Lett. **101**, 237601 (2008).

[50] N. Jaouen, A. C. Dhaussy, J. P. Itié, A. Rogalev, S. Marinel, and Y. Joly, High-pressure dependent ferroelectric phase transition in lead titanate, Phys. Rev. B **75**, 224115 (2007).

[51] S. G. Jabarov, D. P. Kozlenko, S. E. Kichanov, A. V. Belushkin, B. N. Savenko, R. Z. Mextieva, and C. Lathe, High-pressure effect on the ferroelectric-paraelectric transition in $PbTiO_3$, Phys. Solid State **53**, 2300 (2011).

[52] M. Veithen and P. Ghosez, First-principles study of the dielectric and dynamical properties of lithium niobate, Phys. Rev. B **65**, 214302 (2002).

[53] K. Toyoura, M. Ohta, A. Nakamura, and K. Matsunaga, First-principles study on phase transition and ferroelectricity in lithium niobate and tantalate, J. Appl. Phys. **118**, 064103 (2015).

[54] I. A. Kornev, L. Bellaiche, P. Bouvier, P.-E. Janolin, B. Dkhil, and J. Kreisel, Ferroelectricity of perovskites under pressure, Phys. Rev. Lett. **95**, 196804 (2005).

[55] L. E. Cross, A. Fouskova, and S. E. Cummins, Gadolinium molybdate, a new type of ferroelectric crystal, Phys. Rev. Lett. **21**, 812 (1968).

[56] G. Lucazeau, P. Bouvier, A. Pasturel, O. Le Bacq, and T. Pagnier, High-Pressure Study of $Gd_2(MoO_4)_3$ by Raman scattering and *ab initio* calculations, Acta Phys. Pol. A **116**, 25 (2009).

[57] G. Lucazeau, O. Le Bacq, A. Pasturel, P. Bouvier, and T. Pagnier, High-pressure polarized Raman spectra of

Gd$_2$(MoO$_4$)$_3$: phase transitions and amorphization, J. Raman Spectrosc. **42**, 452 (2011).

[58] B. B. Van Aken, T. T. M. Palstra, A. Filippetti, and N. A. Spaldin, The origin of ferroelectricity in magnetoelectric YMnO$_3$, Nat. Mater. **3**, 164 (2004).

[59] S. H. Jabarov, N. T. Dang, S. E. Kichanov, D. P. Kozlenko, L. S. Dubrovinsky, J.-G. Park, S. Lee, A. I. Mammadov, R. Z. Mehdiyeva, B. N. Savenko, N. X. Nghia, L. H. Khiem, N. T. T. Lieu, and L. T. P. Thao, Crystal structure and vibrational spectra of hexagonal manganites YMnO$_3$ and LuMnO$_3$ under high pressure, Mater. Res. Express **6**, 086110 (2019).

[60] D. P. Kozlenko, N. T. Dang, S. E. Kichanov, E. V. Lukin, A. M. Pashayev, A. I. Mammadov, S. H. Jabarov, L. S. Dubrovinsky, H.-P. Liermann, W. Morgenroth, R. Z. Mehdiyeva, V. G. Smotrakov, and B. N. Savenko, Competing magnetic and structural states in multiferroic YMn$_2$O$_5$ at high pressure, Phys. Rev. B **92**, 134409 (2015).

[61] S. P. Ramkumar and E. A. Nowadnick, Octahedral rotations in Ruddlesden-Popper layered oxides under pressure from first principles, Phys. Rev. B **104**, 144105 (2021).

[62] Q. Wang, K. von Arx, D. G. Mazzone, S. Mustafi, M. Horio, J. Küspert, J. Choi, D. Bucher, H. Wo, J. Zhao, W. Zhang, T. C. Asmara, Y. Sassa, M. Månsson, N. B. Christensen, M. Janoschek, T. Kurosawa, N. Momono, M. Oda, M. H. Fischer *et al.*, Uniaxial pressure induced stripe order rotation in La$_{1.88}$Sr$_{0.12}$CuO$_4$, Nat. Commun. **13**, 1795 (2022).

[63] Y.-S. Li, N. Kikugawa, D. A. Sokolov, F. Jerzembeck, A. S. Gibbs, Y. Maeno, C. W. Hicks, J. Schmalian, M. Nicklas, and A. P. Mackenzie, High-sensitivity heat-capacity measurements on Sr$_2$RuO$_4$ under uniaxial pressure, Proc. Natl. Acad. Sci. USA **118**, e2020492118 (2021).

[64] F. Jerzembeck, H. S. Røising, A. Steppke, H. Rosner, D. A. Sokolov, N. Kikugawa, T. Scaffidi, S. H. Simon, A. P. Mackenzie, and C. W. Hicks, The superconductivity of Sr$_2$RuO$_4$ under *c*-axis uniaxial stress, Nat. Commun. **13**, 4596 (2022).

[65] I. Markovia, M. D. Watson, O. J. Clark, F. Mazzola, E. A. Morales, C. A. Hooley, H. Rosner, C. M. Polley, T. Balasubramanian, S. Mukherjee, N. Kikugawa, D. A. Sokolov, A. P. Mackenzie, and P. D. C. King, Electronically driven spin-reorientation transition of the correlated polar metal Ca$_3$Ru$_2$O$_7$, Proc. Natl. Acad. Sci. USA **117**, 15524 (2020).

[66] C. D. Dashwood, A. H. Walker, M. P. Kwasigroch, L. S. I. Veiga, Q. Faure, J. G. Vale, D. G. Porter, P. Manuel, D. D. Khalyavin, F. Orlandi, C. V. Colin, O. Fabelo, F. Krüger, R. S. Perry, R. D. Johnson, A. G. Green, and D. F. McMorrow, Strain control of a bandwidth-driven spin reorientation in Ca$_3$Ru$_2$O$_7$, Nat. Commun. **14**, 6197 (2023).

[67] G. Clarke, D. Daisenberger, X. Luo, S. W. Cheong, N. C. Bristowe, and M. S. Senn, Data for "Pressure-dependent phase transitions in hybrid improper ferroelectric Ruddlesden-Popper oxides", https://doi.org/10.6084/m9.figshare.17136548 (2024).